

Structure and Topology of Phase-Change Telluride Melts

Matthieu Micoulaut¹ and Christophe Bichara²

The structural properties of a germanium telluride melt GeTe_4 are investigated with first principles molecular dynamics simulations. These telluride systems, although different from Ge-rich alloys which are used in phase-change applications, are also potential candidates for such applications. Pair correlation functions and coordination numbers are computed for various temperatures and highlight the fact that the liquid has already some defect octahedral features which are usually found at lower temperatures. A comparison with elemental liquid Te is also provided.

1. Introduction

Phase change materials have received huge attention in recent years, with various technological applications ranging from optical discs, such as CD-RW or DVD-RW discs to Phase-change memory (PRAM) devices, the latter being a promising candidate for future non-volatile computer memory.¹⁻³ In fact, prototype PRAM devices have demonstrated higher density and faster write times than flash memory.⁴ In both applications, the difference in electronic and optical properties between the crystalline and amorphous phase of the materials is at play. For optical storage, the crystalline phase is first hit by a nano-second light pulse from a high intensity “write” laser inside the drive. This brings about a local (sub-micron) melting leading to amorphisation upon cooling thus changing its reflectivity. A different pulse level may reverse the changes, thus erasing the recorded information by recrystallisation of the amorphous phase. A secondary “read” laser with less power will avoid melting and is used to measure the local reflectivity in order to detect if a bit is “on” (locally amorphous, low reflectivity) or “off” (locally crystalline, high reflectivity). PRAM uses the same principle but thermal induced changes between the crystalline and amorphous phases this time result from Joule heating through electrical currents.⁵

In this respect, a crucial question deals with an appropriate choice of material and material properties such as recrystallisation speed, optical, volume or resistivity contrast between the crystalline and amorphous phases. This has led to the creation of a very active field of research and to a series of investigations for PCM applications in basic and applied science. The class of materials on which focus has been placed are the chalcogenides because they display some remarkable properties that can be used for PCM design with appropriate functionalities: low glass transition temperature, large differences in structure between the crystalline and amorphous phases arising from the presence of a lone electronic pair, low band gap, stability of the crystalline and amorphous phases, and different optical and electrical properties.⁶ One should note, however, that other compounds have now been identified for the same kind of applications: organogermanium alloys (IBGe, TDMAGe)⁷ or metalorganics of antimony and tellurium.⁸

In Ge-Sb-Te alloys, three interesting compositional zones for phase change applications have been identified:⁹ a pseudo-tie line with composition $\text{GeTe-Sb}_2\text{Te}_3$, a tellurium deficient zone around GeSb_6 and compositions close to Sb_2Te_3 . Compositional changes lead to drastic changes in material properties¹⁰ and therefore in

¹ Laboratoire de Physique Théorique de la Matière Condensée, Université Pierre et Marie Curie, Boite 121 4, place Jussieu, 75252 Paris Cedex 05, France
mmi@lptl.jussieu.fr

² Centre Interdisciplinaire de Nanoscience de Marseille, CNRS et Université d'Aix-Marseille, Campus de Luminy, Case 913, 13288 Marseille, France

possibilities for PCM applications. For instance, increasing the germanium content along the GeTe-Sb₂Te₃ join will lead to an increase of the melting point¹¹ and a glass transition temperature favouring data retention, but to a decrease of the crystallization speed and the data transfer rate. In the opposite direction, Sb₂Te₃ rich materials will have less stability because of a low activation energy for recrystallisation.¹² The structure of GeSbTe systems has been studied by several experimental techniques¹³ and also by First Principles Molecular Dynamics.¹⁴ It has been shown the c-GeSbTe can be found under two possible configurations hexagonal and a metastable face centered cubic (FCC).¹⁵ Under rapid crystallization however, it has been shown to have a distorted rocksalt structure.¹⁶ These differences are partly due to the increased electronic delocalization of tellurium (Te has an extra lone pair) that leads to local structures in the amorphous phase that can certainly not be determined from the crystalline counterpart, a situation in sharp contrast with lighter chalcogenides such as sulphides and selenides.¹⁷

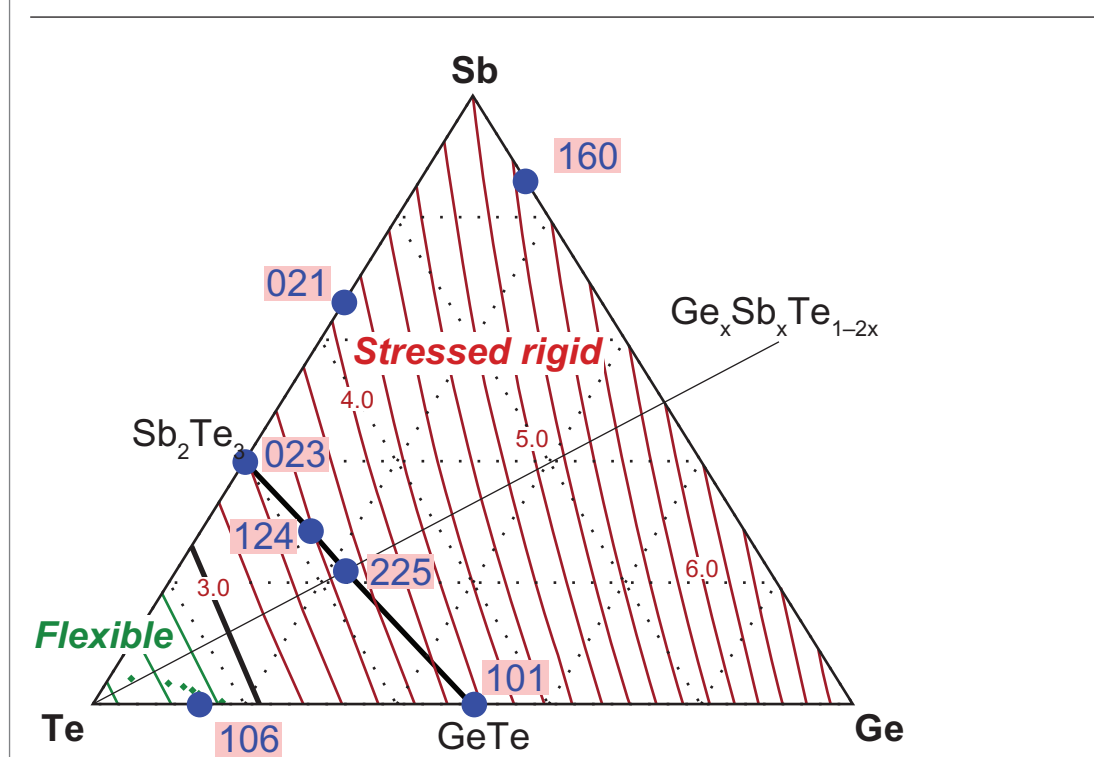
In related binary systems, the focus has mainly been on the phase-change composition Ge-Te system.¹⁸ GeTe exhibits a rock-salt structure at high

temperatures above 400 °C,¹⁹ consisting of two fcc sublattices shifted by half the lattice parameter in each direction with respect to each other. Each sublattice is occupied by either germanium or tellurium. At lower temperatures, a metastable rocksalt structure is found, resulting from the annealing of amorphous thin films. Different authors have reported both experimental and modeling results on this compound. In the liquid and the amorphous phase, Akola and Jones²⁰ have used ab initio Molecular Dynamics to characterize the structure which result in 3-fold coordinated tellurium and fourfold coordinated Ge having either tetrahedral or octahedral bonding sites. Similar simulations have been carried out by Bichara et al.²¹ on GeTe₆ to understand the origin of the observed density anomaly.²²

However, experimental studies from high energy diffraction measurements for different compositions in the binary Ge-Te system have shown that there were very little differences in the pattern of the structure factors,²³ thus making a definite conclusion on structural changes induced by Ge concentration rather difficult.

Certain compositions have been also analyzed in terms of topological constraints derived

Figure 1: Compositional triangle in the Ge-Sb-Te system.²⁹ Contourplot of the number of topological constraints defining a stressed rigid phase (red) and flexible phase (green). According to MD-based constraint counting, a flexible to rigid transition is expected close to the SbTe₄-GeTe₄ join. Green dots are bulk glass compositions.



from rigidity theory.²⁴ In the latter, relevant interactions such as bond-bending and bond-stretching forces are identified with mechanical constraints in very much the same fashion as the pioneering work on trusses by Maxwell.²⁵ The balance between these constraints and the atomic degrees of freedom allows for the definition of compositional regions having a well defined mechanical character. For low connected amorphous networks which are flexible, there are less constraints (interactions) than degrees of freedom so that low energy (floppy) modes can locally deform the network.²⁶ On the opposite side, stressed rigid amorphous systems are obtained if the number of constraints is larger than the number of degrees of freedom. Between the flexible and the stressed rigid phase, an intermediate stress-free (isostatic) phase has been discovered in recent years.²⁷ Details of the phenomenology can be found in Reference.²⁸

According to the theory and given the estimation of bond-bending and bond-stretching constraints from ab initio Molecular Dynamics,²⁹ it was found that the number of constraints per atom in GeTe is equal to $n_c = 3.87$, i.e. it is greater than the number of degrees of freedom in 3 dimensions. Amorphous GeTe can therefore be considered as stressed rigid, whereas a Te rich composition GeTe₆ was found to be flexible ($n_c = 2.73$). It is therefore

tempting to ask if the addition of tellurium into a stressed rigid GeTe system will soften the network backbone, and where the exact location of the flexible to stressed rigid transition can be found in the germanium tellurides. There is some additional experimental evidence which suggests that a flexible to rigid transition takes place in the binary Ge-Te system. Thermodynamic data in the liquid phase show indeed that such alloys display anomalies²² (compressibility maximum, molar volume minimum,...) which bear some striking analogies to what is obtained in isostatic network glasses.³⁰

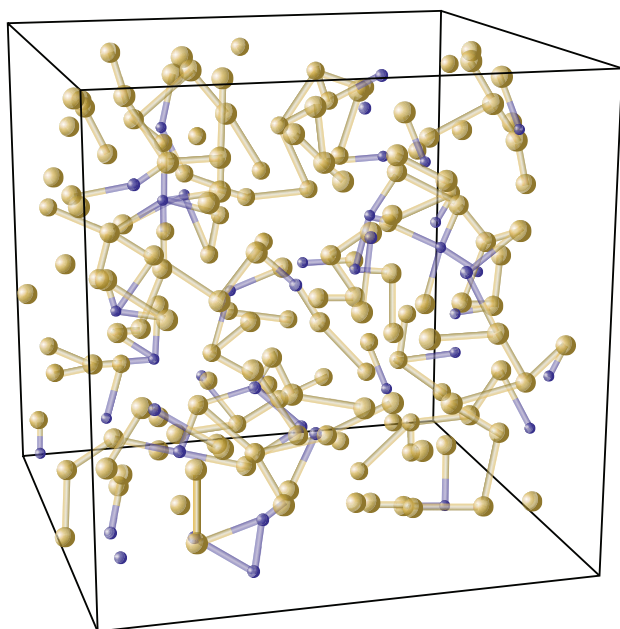
In this contribution, we consider the case of the binary GeTe₄ which should be found in the vicinity of a rigidity transition. In the selenide analog where germanium is always found in a tetrahedral environment, one has exactly $n_c = 3$ from a mean-field constraint counting at $x = 20\%$ germanium,²⁴ i.e. for GeSe₄. We analyze the structural properties of the high temperature liquid, and show that the system is already in a distorted octahedral geometry for the Ge environment, as highlighted by the bond angle distribution, whereas Te is found to have a majority of 1-, 2- and 3-fold coordinated species. A comparison with liquid tellurium is provided. Topological constraints are already present in the liquid and their number suggest that the dominant structural motif for Ge is the defect octahedral geometry.

2. Numerical details

Simulations have been performed at constant volume on a system consisting of 200 atoms. A periodically repeated cubic cell of different sizes was used. The size of the cubic cell was chosen to correspond to a linear extrapolation of the experimental volume data at high temperature.²² The electronic structure was described within Density Functional Theory and evolved self-consistently during the motion. Valence electrons were treated explicitly, in conjunction with norm-conserving pseudopotentials of the Trouiller-Martins type³¹ to account for core-valence interactions. Perdew-Burke-Ernzerhof (PBE) pseudopotentials were used for the exchange-correlation energy.³² The wave functions were expanded at the Γ point of the supercell on a plane-wave basis set defined by an energy cutoff of 20 Ry.

The starting configuration was a 200 atom GeSe₄³³ where all selenium atoms were first replaced by tellurium to generate the GeTe₄ starting configuration. We used a fictitious electron mass of 200 a.u. (in units of $m_e a_0^2$ where m_e is the electronic mass and a_0 is the Bohr radius), and a time step of

Figure 2: A snapshot of the 200 atom liquid GeTe₄ at 1400 K. Note the presence of 2- and 3-fold tellurium along chains.



$\Delta t = 0.1$ fs to integrate the equations of motion. Temperature control has been implemented for both ionic and electronic degrees of freedom by using Nosé-Hoover thermostats. The loss of initial configuration was carried out at 2500 K over a time interval of 25 ps. We then carried out simulations at 2500 K, 2200 K, 2000 K, 1700 K and 1400 K, each over 25 ps. The same procedure was used to simulate elemental tellurium. Computations were performed from statistical averages taken after discarding an initial segment of 2 ps.

3. Pair distribution functions

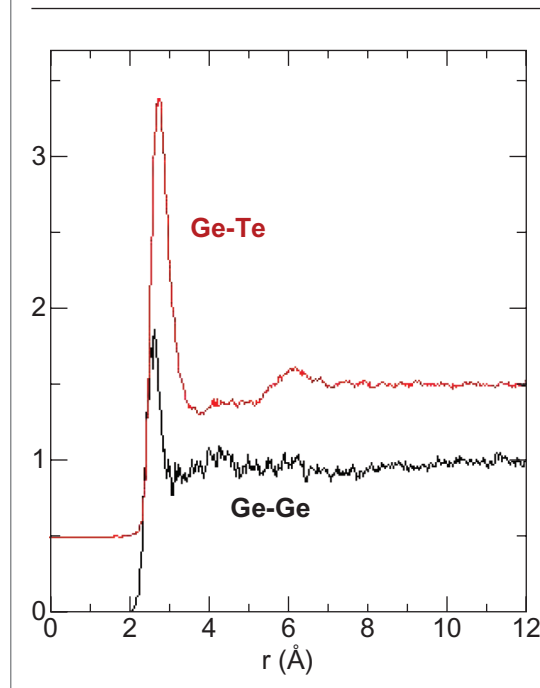
In Figures 3 and 4, we display the calculated pair distribution $g_{ij}(r)$ for different temperatures in the liquid GeTe_4 . For 1400 K, a main peak in Ge-Ge correlations is found close to 2.63 Å, the intensity of this peak being an increasing function with temperature decrease. The remaining global shape of the function, however, does not evolve much with temperature. For the Ge-Te pair distribution function, we find the position of the main peak at 2.74 Å. The latter value is found to be close to the one obtained in GeTe_6 from ab initio simulations (2.78 Å) at lower temperatures^{34,35} but it should be mentioned that the shape of the experimental pair distribution function is very sensitive to temperature as the height and the position of the main peak (i.e. mostly the Ge-Te bond

length) change substantially with a temperature decrease (2.71 Å and 2.84 Å for 663 K and 873 K respectively).^{34,20}

However, as stressed in,³⁵ in GeTe_6 the pair distribution function is also sensitive to structural changes related to changes in the Te-Te correlations. Figure 4 shows that structural changes induced by the Ge concentration are encoded in the Te-Te pair distribution function. At $x = 0$ (liquid Te), we find a main peak at 2.93 Å which shifts to higher r (2.99 Å for GeTe_4) as the Ge composition is increased. Simultaneously, the secondary peak which is identified with the interchain distance is found here to be of 4.2 Å (against 3.2–3.7 Å in liquid Te, depending on the temperature). Thus the addition of germanium leads to an increase of the interchain distance although the overall density change driven by the addition of Ge decreases.²³ Also, since Ge cross-linking induces additional disorder between the pure Te chains, it leads to a broadening of the secondary peak.

The contribution to the pair distribution function can be detailed by looking at nearest neighbour distributions of Te (Figure 5) which show that at the pdf minimum, one has up to four neighbouring atoms. On the other hand, we find that the height of the first two distributions is somewhat higher than the other distributions, indicating of the preminent contribution of the first two neighbours with respect to the interchain distance found at 3.2 Å. When elemental Te is compared to the GeTe_4 , one finds a global shift to lower distances for all distributions (broken lines in Figure 5).

Figure 3: Pair distribution functions Ge-Ge and Ge-Te in the GeTe_4 liquid at 1400 K.



4. Coordination numbers and bond angles

A simple inspection of the bond distances shows already that the liquid cannot be of the same tetrahedral nature as other group IV chalcogenides (e.g. GeSe_4). In fact, a perfect tetrahedron $AX_{4/2}$ has a distance ratio $\delta_{AX} = d_{AX}/d_{XX}$ equal to $\sqrt{3}/8 = 0.61$, a value that is found in experimental and/or simulated silica³⁵ ($\delta_{\text{SiO}_2} = 0.62$) or germania³⁶ ($\delta_{\text{GeO}_2} = 0.62$), and also in other chalcogenides such as GeSe_2 ($\delta_{\text{GeSe}_2} = 0.63$),³⁷ where tetrahedral ordering prevails. For the present GeTe_4 , we find $\delta_{\text{GeTe}_4} = 0.92$, i.e. substantially higher than for oxides and selenides, underscoring the strong deviation from a pure sp^3 hybridization. The latter value of the distance ratio appears to be comparable to densified silicas and germanias for which a tetrahedral to octahedral conversion under pressure occurs.³⁵

Figure 6 shows the bond angle distributions (BADs) Te-Ge-Te and X-Te-X ($X = \text{Ge, Te}$) that provide additional information on the liquid

Figure 4: Left: Te-Te pair distribution function (pdf) in liquid GeTe_4 and Te. Right: Same quantity ($g_{\text{Te-Te}}$) for GeTe_4 with changing temperature.

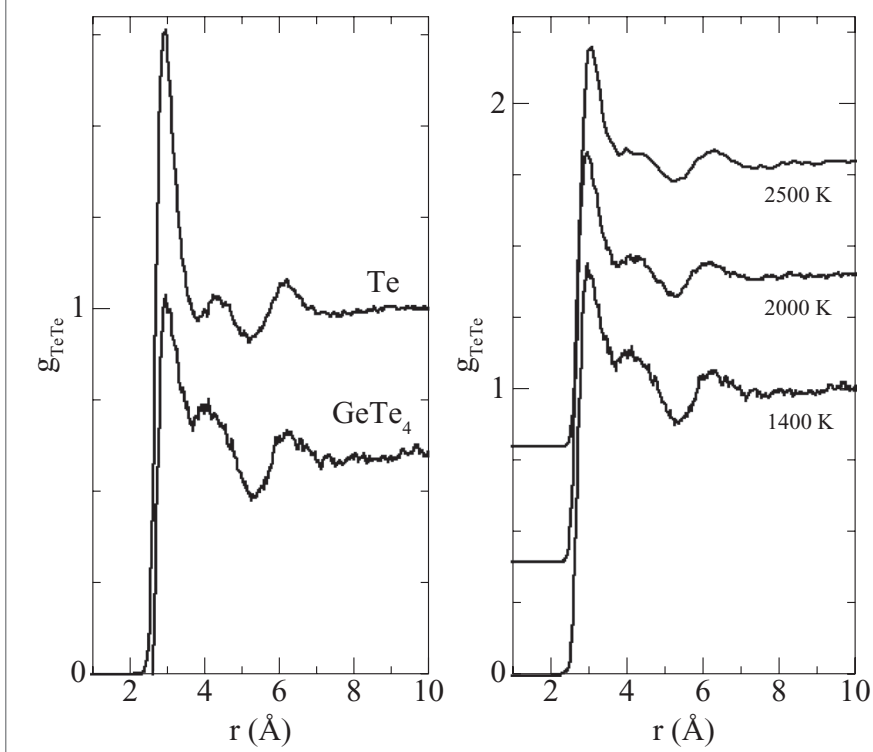


Figure 5: Nearest-neighbour distributions (up to 9) in liquid (1400 K) Te (solid line) and GeTe_4 (broken lines). The thick lines are the corresponding pair distribution function, and equals the sum of the 9 distribution. Red distributions are found after the first pdf minimum.

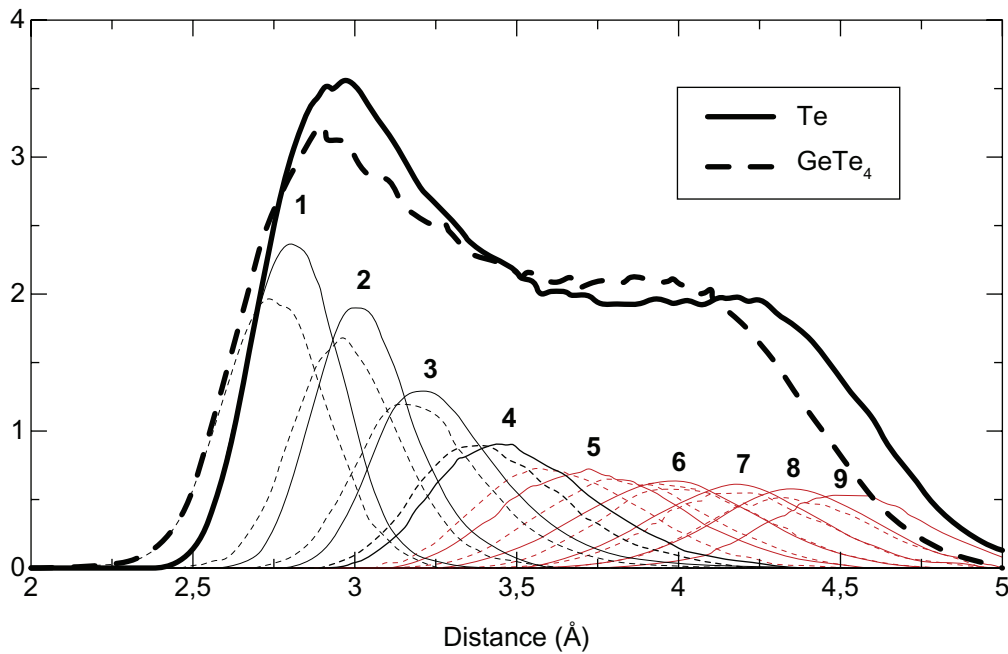
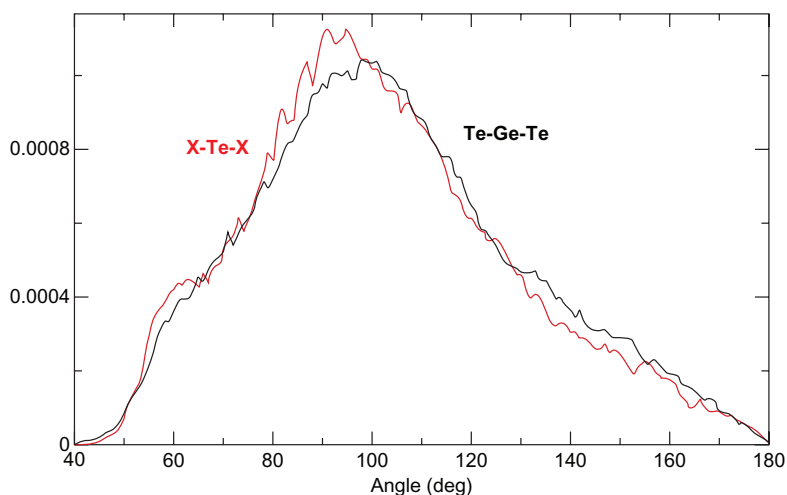


Figure 6: Bond angle distribution in liquid (1400 K) GeTe₄.

topology. Here one can conclude that part of the atoms have a coordination number that is larger than four as the distributions peak at 90°, which is similar to what is expected when (defect) octahedra are present in the structure. The Te-Ge-Te BAD displays two distinct contributions having a clear maximum at around 90°–100° and a contribution somewhat lower than 180°, suggesting that tellurium atoms can lie either in an equatorial plane (90°) of a Ge polyhedra or at its vertices (180°). The present local structure definitely does not display a full tetrahedral character which should manifest by a BAD maximum at around 109°, a feature observed in silica,³⁵ GeO₂³⁸ or in simulated GeSe₂.³⁹ Here, with a maximum found around 100° (i.e. between 90° and 109°), we anticipate (see below) that the structure of the liquid GeTe₄ should be made of 4-fold (partially tetrahedral) and higher coordinated species in an octahedral environment. These results contrast with the BAD related to tellurium (red curve) which has a distribution clearly centered at 90°, indicative of a defect octahedral arrangement.

Further insight into the network topology can be obtained from detailed statistics of *r*-fold coordinated species. The results are displayed in Table I for a cut-off distance of 3.07 and 3.25 Å for Ge and Te respectively (i.e. close to the first minimum in the Ge-Te pair correlation function). We first remark that the liquid at any temperature is made of a majority of 3-fold Ge atoms (about 40%) with a large amount of 2- and 4-fold species, whereas tellurium has mostly two-fold species with also terminal Te (1-fold) and cross-linking Te (*r* = 3). Furthermore one notices

Table I: Fraction (in %) of *r*-coordinated species around Ge and Te atoms in liquid GeTe₄. *r_c* is the cut-off distance used for the calculation.

		<i>r</i> = 1	<i>r</i> = 2	<i>r</i> = 3	<i>r</i> = 4	<i>r</i> = 5	<i>r_c</i>
Ge	1400 K	3.4	18.1	40.2	32.0	6.3	3.07 Å
	1700 K	6.9	27.4	39.0	22.8	3.9	3.07 Å
	2000 K	5.8	26.3	39.8	23.6	4.5	3.07 Å
	2200 K	4.9	23.5	39.7	25.9	6.0	3.07 Å
	2500 K	8.1	29.0	38.4	20.8	3.7	3.07 Å
Te	1400 K	12.7	43.7	32.7	9.8	1.1	3.25 Å
	1700 K	13.7	42.5	32.6	9.5	1.1	3.25 Å
	2000 K	14.7	42.8	32.3	9.1	1.1	3.25 Å
	2200 K	15.2	42.6	31.7	9.2	1.3	3.25 Å
	2500 K	16.1	42.4	31.0	9.2	1.2	3.25 Å

that the distributions are weakly sensitive to temperature changes as the various fractions do not evolve much with temperature. However, at the lowest temperature, we obtain a significant increase of four-fold germanium, whose fraction increases from 22.8% at 1700 K to 32% at 1400 K. This increase is balanced with a decrease of the fraction of 2-fold germanium. On the opposite side, tellurium appears to be rather stable under temperature change with nearly constant statistics, as also highlighted by the fact that the Te-Te pair distribution function is almost identical between 1400 K and 2500 K (Fig. 4, right panel). This suggests that the observed increase of the Te coordination number at lower temperatures⁴⁰ is already fulfilled when the system reaches these higher temperatures (1400 K).

There is no evidence for homopolar Ge-Ge bonds which are found to be less than 1%.

5. Topological constraints

We can analyze in more detail the link between topology and rigidity of the GeTe₄ liquid by computing bond-stretching and bond-bending constraints from the atomic scale trajectory, and following exactly the method proposed in Ref.,²⁹ which has also been applied to other amorphous systems such as Ge-Se glasses⁴¹ and silicates.⁴² We recall here the basic ideas.

If one follows rigidity theory, the first task is to identify relevant interatomic forces between atoms, similar to what Maxwell pioneered for trusses and macroscopic structures.⁴³ In mechanical engineering, the Maxwell stability criterion of macroscopic structures is obtained by equating the number of forces acting on a node of the structure (i.e. the number of bar tensions connecting the node, on the number of Lagrangian constraints) and its number of degrees of freedom. As mentioned above, a similar analysis applied to covalent amorphous networks using

bond-stretching (BS) and bond-bending (BB) interactions as constraints leads to the Phillips-Thorpe rigidity transition^{25,26} which is exactly equal to the Maxwell stability criterion for isostatic structures. As in standard mechanics however, instead of treating the forces and inquiring about motion, one can treat the opposite problem and relate motion to the absence of a restoring force. This is the central concept of the constraint counting procedure from Molecular Dynamics. From the atomic scale trajectories, we apply a structural analysis in relation with topological constraints as defined in rigidity theory.

We consider the six first neighbours around a central atom and sort them according to their distance. The analysis of the corresponding distributions provides an estimation of the number of neighbours, and hence the number of BS constraints. The number of bond-bending constraints is far less immediate to determine, and needs the definition of partial bond angle distributions (PBAD): for each type of a central atom i , the N first neighbours (in the following, $N=6$) are selected and the $N(N-1)/2$ corresponding angles i_0j ($i = 1..5, j = 2..6$) are calculated, i.e. 102, 103, ... 203, etc. The estimation of the second moment of each PBAD gives a quantitative estimate about the angular excursion around the mean angle, thus

measuring the strength of the BB restoring force. Angles displaying a wide excursion are expected to have their corresponding BB constraint broken as there is only weak interaction to maintain a fixed mean angle, whereas sharp bond angle distributions lead to intact constraints.

In the present case, since we deal with liquids, one would expect that most of the constraints are broken by thermal activation, as suggested in.⁴⁴ However, one can still capture salient features, and anticipate the global constraint behaviour at lower temperatures. Figure 7 shows such results extracted from the neighbour distribution for the liquid at 1400 K. The figure represents the first (i.e. mean or peak position, insert) and second moments of each distribution such as those displayed in Fig. 5. Here, one can remark that there is no separation between the first and second shell of neighbors as the peak position steadily increases along with the neighbour rank. However, the radial excursion between two neighbouring atoms already shows features which are close to what is obtained in the amorphous phase for other compositions,²⁹ i.e. Te has only two neighbours having a small standard deviation (of the order of 0.17 Å) with a significant gap separating the standard deviation of the other neighbour distributions (at 0.25 Å), whereas germanium atoms have 3 small standard deviations. A fourth one (at $\sigma_r = 0.2$ Å) is intermediate, and may contribute to bond-stretching constraints at lower temperatures. The latter behaviour appears therefore to be rather similar to what has been obtained in liquid silicates where it was shown that the constraint of the fourth neighbour of a Group IV atom (i.e. oxygen around silicon) is the most sensitive to temperature change.⁴²

Results concerning the BB constraint estimate are given in Fig. 8 and 9. From the former representing the Ge-centred PBADs, we can clearly conclude that some angles display a small excursion around the mean angle of 100° (colored curves) as compared to the other distributions. The standard deviation of these distributions are represented in Fig. 9 as a function of an arbitrary angle number ranging from 1 to 15 as we have chosen up to $N = 6$ possible neighbours for the calculation of the PBADs (and thus $N(N-1)/2 = 15$ PBADs).

The features found appear to be rather similar to what has been obtained in Ge-Sb-Te materials,²⁹ i.e. although Te has a coordination number larger than 2, it will give rise to only one constraint at a lower temperature. In Fig. 9, one can indeed notice that there is a clear gap between the standard deviation $\sigma_1 = 26^\circ$ of angle

Figure 7: Radial standard deviation (second moment) and neighbour peak position (first moment, insert) in the 1400 K liquid GeTe_4 for Te and Ge atoms.

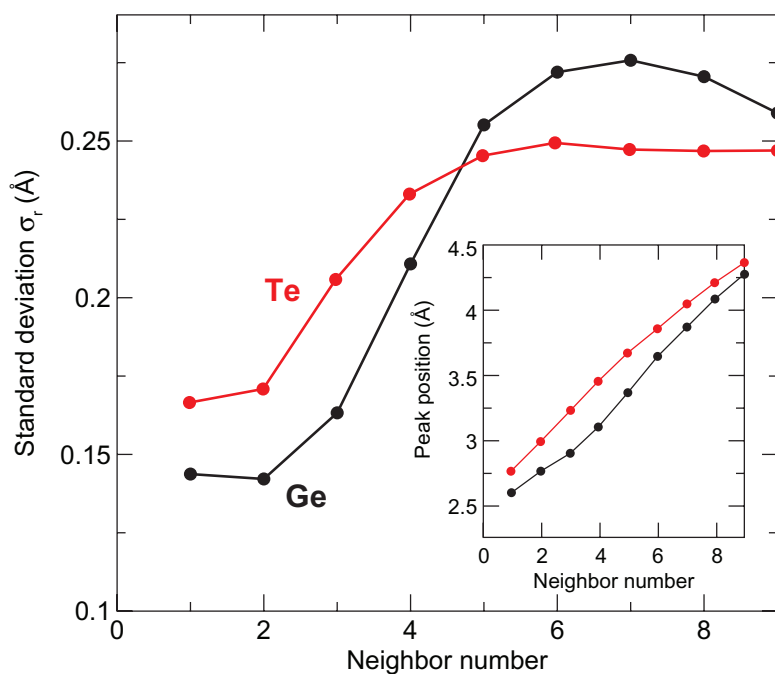


Figure 8: 15 partial bond angle distribution around Ge atoms in liquid GeTe₄ at 1400 K (here for an arbitrary N = 6). The colored curves correspond to distributions having a low standard deviation (i.e. probable intact constraints at lower temperatures). Broken curves represent the 12 remaining ones.

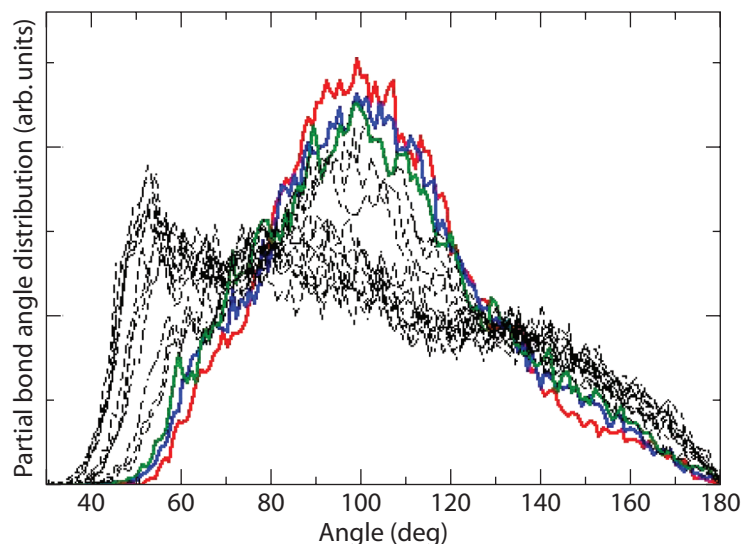
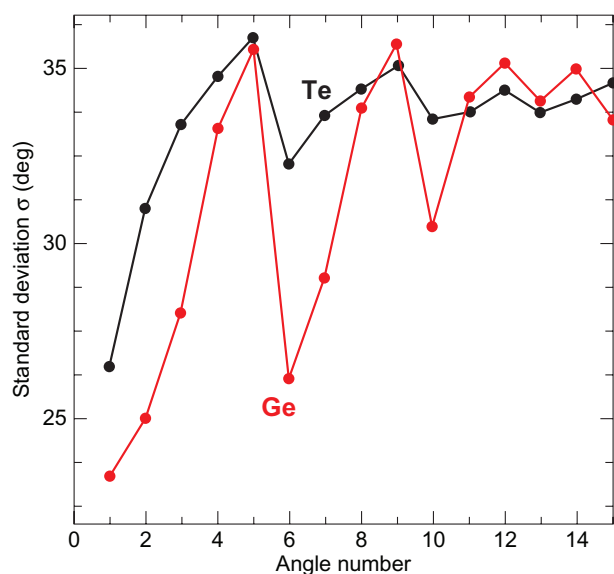


Figure 9: Standard deviation of Ge (red) and Te-based (black) PBADs as a function of the angle number in liquid (1400 K) GeTe₄.



number 1 and all other standard deviations (black curve). The value of σ_1 will steadily decrease as the temperature is decreased.⁴² Similarly, we can state that BB constraints for the Ge atom (red curve in Fig. 9) should be about 6 (six standard deviations having $\sigma_1 < 30^\circ$). However, we remark that angles

involving the fourth Ge neighbour (angles 3, 7 and 11) have a larger standard deviation, in agreement with the fact that the radial excursions involving this neighbour are larger (Fig. 7). The same analysis at lower temperatures should allow for a clear understanding of the non-equivalent angular excursion found for the six angles. In fact, it has been demonstrated that such a non-equivalent angular excursion was a feature of stressed rigidity.⁴¹

Summary and conclusions

In this contribution, we have investigated from First Principles Molecular Dynamics the structural properties of GeTe₄ high temperature liquids. These systems are found close to an expected flexible to rigid transition whose location should differ when compared to their selenide counterpart.

Results show that the GeTe₄ liquid is made of a majority of 2 and 3-fold tellurium atoms, and 3- and 4-fold Ge atoms. Concerning the latter, bond angle distributions suggest that the local geometry is octahedral with defects as contributions close to 90° and 180° are found. A minor fraction for higher coordinated (five-fold) germanium is obtained. These results are found to be nearly temperature independent although changes in the local topology are observed at the lowest temperature. An analysis from rigidity theory shows the premise of what is expected at a low temperature for a fully connected amorphous network, i.e. one and six bond-bending constraints for Te and Ge respectively.

With these results in hand and once the system is quenched to an amorphous state, one should be able to compute the corresponding constraints used for the understanding of compositional trends in telluride glasses where the 8-N rule does not apply. In this respect, they should be helpful in describing more complex telluride materials for electrical switching applications^{45,46} where rigidity effects have also been observed.

Received 8 July 2011.

References

1. S. Raoux, W. Welnic, D. Ielmini, *Chem. Rev.* 110, 240 (2010).
2. D. Lencer, M. Salinga, B. Grabowski, T. Hickel, J. Neugebauer, M. Wuttig, *Nature Mat.* 7, 972 (2008).
3. *Phase Change Materials and Applications*, S. Raoux, M. Wuttig Eds. (Springer, 2008).
4. A. Kolobov, P. Fons, J. Tominaga, T. Uruga, *J. Non-Cryst. Solids* 352, 1612 (2006).
5. A. Pirovano, A.L. Lacaita, A. Benvenuti, F. Pellizzer, R. Bez *IEEE Trans. Electron Devices* Vol. 51, No. 3, 452 (2004).
6. A.V. Kolobov, P. Fons, A.I. Frenkel, A.L. Ankudinov, J. Tominaga, T. Uruga *Nature* 3, 703 (2004).

7. M. Bosi, G. Attolini, C. Ferrari, C. Frigeri, J.C. Rimada Herrera, E. Gombia, C. Pelosi, R.W. Peng, *J. Crystal Growth*, 310, 3282 (2008).
8. X. Shi, M. Schaekers, F. Leys, R. Loo, M. Caymax, R. Brus, C. Zhao, B. Lamare, E. Woelk, D. Shenai, *ECS Trans.* 3, 849 (2006).
9. M. Wuttig, N. Yamada, *Nature Mat.* 6, 824 (2007).
10. A. Klein, C. Steimer, H. Dieker, B. Späth, P. Fons, A. Kolobov, M. Wuttig: *Phys. Rev. Lett.* 100, 016402 (2008).
11. E. Morales-Sánchez, E.F. Prokhorov, A. Mendoza-Galván, J. González-Hernández, *J. Appl. Phys.* 91, 697 (2002).
12. J. Yu, B. Liu, T. Zhang, S. Feng, B. Chen, *Appl. Surface Science* 253, 6125 (2007).
13. D. A. Baker, M.A. Paessler, G. Lucovsky, S.C. Agarwal, P.C. Taylor, *Phys. Rev. Lett.* 96, 255501 (2006)
14. C. Bichara, M. Johnson, J.-P. Gaspard, *Phys. Rev. B* 75, 060201 (2007); S. Caravati, M. Bernasconi, T.D. Kuehne, M. Krack, and M. Parrinello, *Appl. Phys. Lett.* 91, 171906 (2007); J. Akola, R.O. Jones, *Phys. Rev. B* 76, 235201 (2007).
15. T. Matsunaga, N. Yamada, *Phys. Rev. B* 69, 104111 (2004).
16. K. Rabe, J.D. Joannopoulos, *Phys. Rev. B* 36, 6631 (1987).
17. D.G. Georgiev, P. Boolchand, M. Micoulaut, *J. Optoelectr. Adv. Mater.* 4, 823 (2002).
18. Y. Kawakita, Y. Kato, S. Tahara, H. Fuji, S. Takeda, K. Maruyama, *J. Non-Cryst. Solids* 353, 1999 (2007).
19. K.M. Rabe, J.D. Joannopoulos, *J. D. Phys. Rev. B* 36, 6631 (1987).
20. J. Akola, R.O. Jones, *Phys. Rev. Lett.* 100, 205502 (2008).
21. R. Shaltaf, E. Durgun, J.-Y. Raty, Ph. Ghosez, X. Gonze, *Phys. Rev. B* 78, 205203 (2008).
22. Y. Tsuchiya, *J. Phys. Soc. Japan* 60, 227 (1991).
23. K. Ichikawa, Y. Kameda, Q. Xu, M. Misawa, *J. Non-Cryst. Solids* 95–96, 185 (1987).
24. M. Micoulaut, J.C. Phillips, *Physical Review B* 67, 104204 (2003).
25. J.C. Phillips, *J. Non-Cryst. Solids* 34, 153 (1979).
26. M.F. Thorpe, *J. Non-Cryst. Solids* 57, 355 (1983).
27. D. Selvenathan, W.J. Bresser, P. Boolchand, *Phys. Rev. B* 61, 15 061 (2000).
28. Rigidity and Boolchand Intermediate Phases in nanomaterials, M. Micoulaut, M. Popescu Eds. INOE, Bucarest, 2009.
29. M. Micoulaut, C. Otjacques, J.-Y. Raty, C. Bichara, *Physical Review B* 81, 174206 (2010).
30. C. Bourgel, M. Micoulaut, M. Malki, P. Simon, *Phys. Rev. B* 79 024201 (2009).
31. N. Trouillier, J.L. Martins, *Phys. Rev. B* 43, 1993 (1991).
32. J.P. Perdew, K. Burke, M. Enzerhof, *Phys. Rev. Lett.* 77, 3865 (1996).
33. C. Massobrio, M. Celino, P.S. Salmon, R.A. Martin, M. Micoulaut, A. Pasquarello, *Phys. Rev. B* 79 174201(1–8) (2009).
34. C. Bichara, M. Johnson, J.-Y. Raty, *Phys. Rev. Lett.* 95, 267801 (2005).
35. Y. Kawakita, Y. Kato, S. Tahara, H. Fuji, S. Takeda, K. Maruyama, *J. Non-Cryst. Solids* 353, 1999 (2007).
35. M. Micoulaut, *J. Phys.: Condens. Matter* 16, L131 (2004).
36. D. L. Price, M. L. Saboungi, and A. C. Barnes, *Phys. Rev. Lett.* 81, 3207 (1998).
37. P. S. Salmon, *Proc. R. Soc. London, Ser. A* 437, 591 (1992).
38. M. Micoulaut, Y. Guissani, B. Guillot, *Physical Review E* 73 031504(1–11) (2006).
39. C. Massobrio, M. Micoulaut, P.S. Salmon, *Solid State Sciences* 12, 199–203 (2010).
40. A. Menelle, R. Bellissent, A.M. Flanck, *Europhys. Lett.* 4, 705 (1987).
41. M. Bauchy, M. Micoulaut, M. Celino, M. Boero, S. Le Roux, C. Massobrio, *Phys. Rev. B* 83 (2011).
42. M. Bauchy, M. Micoulaut, *J. Non-Cryst. Solids* 357, 2530 (2011).
43. J.C. Maxwell, *Philos. Mag.* 27, 294 (1864); J.L. Lagrange, *Mécanique Analytique* (Paris, 1788).
44. P.K. Gupta, J.C. Mauro, *J. Chem. Phys.* 130 094503 (2009).
45. P. Pattanayak, N. Manikandan, M. Paulraj, S. Asokan, *J. Phys. Cond. Matt.* 19, 036224 (2007).
46. P. Pattanayak, S. Asokan *Solid State. Comm.* 148, 378 (2008).



Matthieu Micoulaut received his Ph.D. in Theoretical Physics from University Paris VI (1993). He is currently Professor in theory of condensed matter (CNRS and UPMC-Paris VI) and chairing the Masters program in Nuclear Engineering at UPMC. His research interests include theoretical aspects of granular gases, glass transition, glasses and amorphous solids, and topology based approaches and molecular simulations for the description of the structure and the dynamics of supercooled liquids.



Christophe Bichara is Research Director at CNRS with an expertise in Computational Materials Science. He graduated in Chemical Engineering and obtained a PhD in Chemical Physics at Aix-Marseille University. His current interest lies in the study of disorder, liquid matter, non crystalline materials as well as the growth mechanisms of carbon nanostructures.